processes

MDPI

Article

Influence of Sodium New *Houttuyfonate* as a New EGFR-TK Inhibitor on the Apoptosis and Autophagy of MCF-7 Cells and Its Toxicity to *Caenorhabditis elegans*

Linsong Yang *, Jia Xu, Yucheng Li, Zilong Gong, Meijun Shi, Jie Zhu and Yucai He *

Biomedicine Laboratory, School of Pharmacy & School of Biological and Food Engineering, Changzhou University, Gehu Road, Wujin District, Changzhou 213164, China; s22090860043@smail.cczu.edu.cn (J.X.); s21091055082@smail.cczu.edu.cn (Y.L.); 20081703009@smail.cczu.edu.cn (M.S.); zhujie@cczu.edu.cn (J.Z.)

* Correspondence: linsongyang@cczu.edu.cn (L.Y.); heyucai2001@163.com (Y.H.); Tel.: +86-519-86334598 (L.Y. & Y.H.)

Abstract: Sodium new *houttuyfonate* (SNH) is volatile oil extracted from *Houttuynia cordata* Thunb. Its molecular formula is $C_{14}H_{27}O_5SNa$, and molecular weight is 330.41. It is a new anti-inflammatory drug that has been used clinically over recent years. In this work, the binding interaction simulation study on SNH and epidermal growth factor receptor-tyrosine kinase (EGFR-TK) was conducted. SNH demonstrated a good binding ability to EGFR-TK and formed hydrogen-bonds with Cys773, Asp776, and Tyr777. This indicated that SNH might play an antitumor role as a potential inhibitor of EGFR-TK. In vitro, after treatment with various doses of SNH for 48 h, the viability of MCF-7 cells was 100.0, 98.23, 83.45, 76.24, 68.53, and 32.24, respectively, accompanied by a concentration increase in SNH. Moreover, cell viability of 250 μg/mL group decreased by more than 30%. Meanwhile, SNH significantly decreased cell cloning ability, and the quantities of clones were 456, 283, 137, and 152 in different groups (0 μg/mL, 100 μg/mL, 200 μg/mL, 250 μg/mL). In addition, SNH of different concentrations promoted the apoptosis of MCF-7 cells, which showed certain morphological characteristics of apoptotic cells including loss of cell adhesiveness, nuclear shrinkage, and appearance of apoptotic bodies. Furthermore, SNH effectively attenuated the migration of MCF-7 cells by decreasing the expressions of NF-kBp65 and vascular endothelial growth factor (VEGF). The increased number of apoptotic cells was also observed through hoechst33258 staining and Annexin V-PI staining, which corroborated with the decreased ratio of Bax and Bcl-2. Moreover, SNH induced the appearance of LC3 positive autophagosomes in MCF-7 cells. In vivo, SNH showed obvious antinematode activity, and LC50 was 40.46 μg/mL. Thus, SNH plays an antitumor role via regulating the apoptosis, autophagy, and migration of MCF-7 cells, and might act as a potential alternative drug in the treatment of breast cancer.

Keywords: sodium new *Houttuyfonate*; apoptosis; migration; autophagy; antinematode

Citation: Yang, L.; Xu, J.; Li, Y.; Gong, Z.; Shi, M.; Zhu, J.; He, Y. Influence of Sodium New *Houttuyfonate* as a New EGFR-TK Inhibitor on the Apoptosis and Autophagy of MCF-7 Cells and Its Toxicity to *Caenorhabditis elegans*. *Processes* **2023**, *11*, 1652. https://doi.org/10.3390/pr11061652

Academic Editor: Carla Silva

Received: 14 April 2023
Revised: 18 May 2023
Accepted: 23 May 2023
Published: 29 May 2023

1. Introduction

Breast cancer mostly occurs in women. The number of female patients with breast cancer among all cancer patients accounts for 11.7%, and the number of breast cancer deaths is up to 6.9% of the total cancer deaths among women [1]. In recent years, its incidence has shown a clear upward trend [2]. Breast cancer is a complicated disease induced by multiple factors such as age, genetic predisposition, breast density [3], obesity [4], hormonal imbalance [5], and mutations [6].

According to a large number of previous studies, the inhibition of cell apoptosis is pivotal to the development of cancer [7]. The mechanism of cell apoptosis is complicated and related to many signal pathways. Among them, The Bcl-2 family group is the principle regulatory member of the apoptosis signal pathway [8]. The Bcl-2 family not only involves apoptotic proteins such as Bak, Bax, Bcl-Xs, etc., but also antiapoptotic proteins such as

Bcl-2, Bcl-w, Mcl-1, BFL-1, and Bcl-XL. The effect of apoptosis closely depends on the release of cytochrome C, the activation of P53, and the ratio of Bax and Bcl-2 [9]. Moreover, NF-κB transcription factor plays a decisive role in regulating cell apoptosis [10], and some studies show that NF-κB directly influences the level of apparent pro-survival factors in the Bcl-2 family, such as Bcl-XL [11]. These findings may contribute to oncogenesis associated with abnormal NF-κB activity [12]. In addition to apoptosis, autophagy is also a clinical strategy to promote the programmed cell death of cancer cells [13–15]. Autophagy widely exists in cells, which is the gradation and recycling process of biological macromolecules in cells. It is indispensable during the processes of cell growth and metabolism [16]. The interaction of apoptosis and autophagy jointly promotes and affects programmed cell death and maintains the body's own steady state and stress response under external environmental stimulation. In the process of cancer treatment, they can play a synergistic relationship to form a dual promoter of cell death [17].

At present, the traditional methods of treating breast cancer consist of surgical resection, radiotherapy, chemotherapy, gene therapy, and endocrine therapy [18,19]. Despite many various curative treatments to deal with breast cancer, the prognosis of patients is still very poor, and side effects exist such as alopecia [20], immunosuppression, and mental illness in women [21]. Thus, it is urgent to find a more efficient and safer treatment for breast cancer. In recent years, more and more Chinese herbal medicines, such as *Taxol* [22], *Astragalus membranaceus* [23], and *Radix seu Herba Marsdeniae Tenacissimae* [24], have been used as antitumor drugs in clinical practice. Chinese herbal medicine is not only positively involved in preventing the development of tumors [25]; it also has the characteristics of raising the quality of life of patients [26], lower cost, and smaller adverse reactions. Phytochemicals have been a focus as a novel, potential anticancer medicine. Currently, it has become a trend to screen and develop effective ingredients from medicinal plants that can be used to treat a number of diseases.

Houttuynia cordata Thunb. (HCT) belongs to the Saururaceae, which grows in a moist and shady environment. Its pharmaceutical properties are universally known among the people of Asia [27]. Many extracts of HCT have been proven to have notable anti-inflammatory effects [28]. When human mast cells were cultured with calcium ionophore, HCT ethanolic extract was found to inhibit the phosphorylation of IκB and decrease the expressions of IL-6, IL-8, and TNF-α [29]. Ethanolic extract of HCT had significant anticancer effects [30]. HCT contains many active ingredients, such as volatile and essential oils, polysaccharides, sodium *houttuyfonate* (SH), and 2-undecanone, were also discovered to have various anti-inflammatory effects. As an active biological molecule isolated from HCT, SH significantly reduce the expressions of TNF-α and IL-1β [31]. Furthermore, SH had the antibacterial, antiviral, and anti-inflammatory activity [32–34]. Sodium new *houttuyfonate* (SNH) is an addition product of dodecanoyl acetaldehyde of volatile oil and sodium bisulfite, which exhibits the same effects as SH but is more stable. In our previous research, SNH showed a significant antitumor effect on HepG2 cells [35]. However, few studies have been reported on the anti-breast cancer effect of SNH in vitro and in vivo. Thus, the regulation of SNH among apoptosis, autophagy, and the migration of MCF-7 cells will be revealed in this study, as well as its molecular mechanisms.

It is known that approximately 30% of human breast tumors overexpress epidermal growth factor receptor (EGFR) [36]. A high level of EGFR promotes the proliferation, angiogenesis, adhesion, invasion, and metastasis of cancer cells, inhibits their apoptosis, and finally results in a low survival rate of tumor patients. When EGFR-tyrosine kinase (EGFR-TK) is over-expressed [37], it would block cell-programmed apoptosis, make cell grow out of control (i.e., always in a proliferative state), and promote the occurrence of malignant tumors. Therefore, EGFR-TK has been a focus as a potential molecular antitumor target [38], and its inhibitor shows good anticancer effect in clinical trials [39].

There are several common features between cancer and diseases caused by parasites. For example, they express some common antigens, such as Tn (CD175), TF (CD176), and sialic Tn (CD175s) antigens [40], and have the ability of unlimited proliferation, antiapopto-

sis, tissue infiltration, and immune escape. More interestingly, antineoplastic drugs and antiparasitic drugs have significant cross effects; thus, their potential interactions can be analyzed [41]. Moreover, due to the increasing need to reduce animal experiments [42], *Caenorhabditis elegans* (*C. elegans*) has become an ideal model organism in vivo for screening anticancer drugs which has no ethics problem [43–45]. More importantly, 60% to 80% of nematode genes are homologous to humans, and many conservative biological processes are similar in them [46].

In this work, the molecular model of SNH was used to dock with the EGFR-TK receptor protein, and the interaction between SNH and the key catalytic residues of EGFR was analyzed; then, the regulation of SNH on the apoptosis, cell clone formation, migration, and autophagy was also analyzed. In addition, the antiparasitic potential of SNH was examined by using *C. elegans* as a parasite model.

2. Materials and Methods

2.1. Materials and Reagents

Sodium new *houttuyfonate* (SNH), an extract of *houttuynia* (Sources: Shanxi Province; Herbarium registration number: XBGH006851; Appraiser: Sifeng Li) whose purity is 97%, was from Xi'an Kailai Biological Engineering Co., Ltd. (Xi'an, China). MCF-7 and Hela cells were donated by Prof. Jie Ren. *C. elegans* and *E.coli* OP50 were donated by Dr. Ziheng Zhuang. DMEM was from Gibco (Waltham, MA, USA). The 3-(4,5-dimethylthiazol-2-yl)-2,5-diphenyl tetrazolium bromide (MTT), penicillin, streptomycin, and TRIzol reagent were purchased from Sigma Chemical Co., Ltd. (St. Louis, MO, USA). Fetal bovine serum (FBS) was from Tian hang Biotech Co. Ltd. (Hangzhou, China). Annexin V-FITC/PI apoptosis detection kit and Hoechst33258 kit were purchased from Shanghai Beyotime Biological Technology Co. Ltd. (Shanghai, China). The primers of GADPH, VEGF, Bcl-2, NF-kBp65, and Bax were provided by Shanghai Sangon Biological Engineering Technology and Service Company (Shanghai, China). Triton X-100, PrimeScript II 1st strand cDNA Synthesis Kit and DNA Taq enzyme were bought from Vazyme Biotech Co., Ltd. (Nanjing, China). Goat serum, HRP Goat Anti Rabbit IgG, FITC labeled goat anti rabbit IgG, color pre-stained protein marker, BCA protein assy kit, and rabbit anti-human polyclonal antibodies of NF-κBp65, VEGF, Bax, Bcl-2, and β-actin were purchased from Boster Biological Technology Co., Ltd. (Wuhan, China). Rabbit anti-human LC3 polyclonal antibody and DAPI staining solution were bought from Beijing Biosynthesis Biotechnology Co., Ltd. (Beijing, China). Other reagents were analytical grade.

2.2. Physicochemical Parameters

The CAS number of the SNH is 1847-58-1. The Wujing database "http://www.basechem.org (accessed on 16 March 2021)" and TOXICOLOGY DATA NETWORK "https://toxnet.nlm.nih.gov (accessed on 16 March 2021) were adopted to obtain various parameters, including molecular weight, octanol/water partition coefficient, toxicity, total polar surface area (TPSA), number of hydrogen bond receptors, number of hydrogen bond donors, and so on. Both databases are comprehensive, professional, dedicated, and free chemical information bases. Calculation of the hydrophobic parameters can be viewed from ChemBioDraw Ultra 14.0 software.

2.3. Docking Study

The ChemBioDraw program served to draw the structure of SNH, and then the latter was imported into the Discovery Studio 2021 software (Biovia DS, Dassault Systemes SE, Vélizy-Villacouplay, France). The preparation of SNH was conducted by Prepare Ligands module, which produces stereoisomers, neutralizes the ligand charged structures, and ionizes the entire structures to a neutral pH7. Docking calculations were executed on SNH (ligands) through the EGFR kinase domain model (Protein code: 1M17.pdb; rcsb.org/3d-view/1M17). The protein was originally subjected to the Prepare Protein panel of DS software. Then, the next step was adding the missing hydrogen atoms, side chains,

and the protons. Using the Receptor–ligand panel, the EGFR kinase composite crystal is additionally configured to produce a sphere associated with the active site surrounded by the ligand. The formation of the sphere shows the active site of the protein, which is over the workspace of the ligand. Then, the small molecular ligands were deleted. The docking method was carried out by applying the one docking method, which was CDOCK module of DS. The force field CHARMm was used. The Docking Preferences parameter was modified to save the first six conformations generated by docking.

2.4. Cell Culture

MCF-7 and Hela cells were growth in DMEM supplemented with 10% FBS, 100 U/mL penicillin, and 100 μg/mL streptomycin, respectively. Cells were cultured in a humidified incubator (SanyoHFU586, Osaka, Japan) with a 5% CO_2 at the temperature of 37 °C. For each run of experiments, cells were thawed, passaged twice, and used in the following experiments.

2.5. MTT Assay

The viability of MCF-7 and Hela cells was analyzed by MTT assay, as previously described [47]. Briefly, the cells were seeded in a 96-well plate at the density of 5×10^3 cells per well. Following incubation for 24 h, DMEM was sucked away and 100 μL of fresh culture medium was placed into each well, which is in the presence of a series of concentrations of SNH (50, 100, 150, 200, and 250 μg/mL). Meanwhile, 100 μL of culture medium was put into the control wells and three replicates were set for each group. After 48 h, 20 μL of 0.5 mg/mL MTT solution was placed into every well, and cells continued to culture for 4 h. Then, the medium was replaced by 100 μL of DMSO. After the crystals in every well were completely dissolved for 15 min, the absorbance at 490 nm was detected on a Microplate Reader (Bio-Rad 550, Hercules, CA, USA).

2.6. Soft Agar Clonogenesis Assay

This experiment was conducted according to the previously described protocol [48]. MCF-7 cells were incubated in 6-well plates with a density of 500 cells per well. After 24 h, the complete medium in the presence of a series of concentrations of SNH was put into each group, respectively. After 48 h, the medium was replaced by fresh medium. Then, the cells continued to be cultivated for 10 more days. During this period, the medium was renewed every 3 days. After 10 days, 4% paraformaldehyde was added to fix MCF-7 cells for 15 min. Then, colonies were stained with 0.5% crystal violet solution. Finally, the stained cell colonies were photographed and counted by image J.

2.7. Annexin V-PI Double Staining

MCF-7 cells were seeded in 6-well plates with a density of 2×10^4 cells per well. After being treated with various concentrations of SNH for 48 h, cells were collected and mixed with 195 μL binding buffer in accordance with the manufacturer's instructions of Annexin V-FITC/PI apoptosis detection kit. Then, cells in each group were exposed to 5 μL of FITC labeled annexin V antibody and 10 μL of PI in the dark for 15 min. Samples were assayed with Flow cytometer (BD FACSCalibur, Franklin Lakes, NJ, USA) independently.

2.8. Hoechst33258 Staining

Hoechst33258, a low-toxicity blue, fluorescent dye, can easily penetrate the cell membrane. Thus, hoechst33258 staining was utilized to analyze the influence SNH on MCF-7 cells apoptosis as previously described [35]. A total of 2×10^4 cells cultured in 6-well plates were exposed to various doses of SNH for 48 h. Subsequently, the MCF-7 cells were fixed for 15 min with 4% paraformaldehyde and then incubated for 5 min with hoechst33258 solution, the concentration of which was 1 μg/mL. Ultimately, the staining was examined through a fluorescence microscope (Nikon C2+, Tokyo, Japan).

2.9. Wound Healing Assay

The migratory ability of MCF-7 cells was tested by a monolayer scratch assay as previously described [49]. Briefly, cells were incubated in a 6-well plate (2.5×10^5 cells/well) and cultured in a humid environment at 5% CO_2 and 37 °C. After the complete contact, the wounds were made using a 10 µL pipette tip and then gently washed three times in order to remove dead or floating cells. Subsequently, 2 mL of DMEM, in the presence of various concentrations of SNH, was put into wells, respectively. Pictures of the wounded area were taken at each time point of 0, 6, 12, 24, 30, 36, and 48 h. The experiment was repeated 3 times.

2.10. RT-PCR

MCF-7 cells were incubated in a 6-well plate with 2.5×10^6 cells per well. After 24 h, cells were processed with 2 mL of 250 µg/mL SNH or DMEM, respectively, for 48 h. The following experimental steps were mainly in accordance with the previously described protocol [47]. Briefly, total RNA of MCF-7 cells was obtained using TRIzol, and then reverse-transcription was conducted by using PrimeScript II 1st strand cDNA Synthesis Kit. Taq DNA Polymerase, dNTP, 10× Taq Buffer, 5× Betaine, 10 pmol of forward and reverse primers, 100 ng of MCF-7 cells' cDNA, and distilled water were mixed and formed a final volume of 10 µL. The sequences of primer and product lengths are shown in Table 1. The reaction started at 94 °C for 2 min; after that, it was followed by 30 cycles of 94 °C for 10 s (denaturation), different annealing temperatures for 20 s which depended on the target gene (55 °C for GADPH, VEGF and Bax, 52 °C for Bcl-2, and 61 °C for NF-kBp65), and by 72 °C for 40 s for chain extension. GADPH was used as an endogenous control. Every sample was conducted in three replicates.

Table 1. Primer sequences for PCR.

Gene	Forward Primer (5′-3′)	Reverse Primer (5′-3′)	Product Size (bp)
GADPH	5′-AGAAGGCTGGGGCTCATTTG-3′	5′-AGGGGCCATCCACAGTCTC-3′	258
VEGF	5′-CGCAGCTACTGCCATCCAAT-3′	5′-CCCACAGGGATTTTCTTGTCTT-3′	288
Bax	5′-TTTGCTTCAGGGTTTCATCC-3′	5′-CAGTTGAAGTTGCCGTCAGA-3′	246
Bcl-2	5′-CACGCTGGGAGAACA-3′	5′-CTGGGAGGAGAAGATG-3′	877
NF-kBp65	5′-GGCCATGGACGAACTGTTCC-3′	5′-GAGGGTCCTTGGTGACCAG-3′	248

2.11. Western Blotting

A total of 5×10^5 MCF-7 cells were cultivated in a 6-well plate and stimulated with different concentrations of SNH for 48 h. The subsequent experiment was conducted as a modified protocol [50]. Briefly, cells were collected and lysed on ice with 100 mL of RIPA buffer containing 1% protease inhibitor for 20 min. Then, the cellular lysate was centrifuged at 12,000 rpm and 4 °C for 10 min. The supernatant was collected, and protein quantification was performed using the BCA method. Sample proteins were separated using 12% SDS-PAGE at 120 V for 30 min. After electrophoresis separation, the protein bands were transferred to the PVDF membrane at 320 mA and 4 °C for 45 min. PVDF membrane was sealed with 5% skimmed milk for 1 h. After rinsing with TBST buffer, rabbit anti-human primary antibodies (1:1000) of Bcl-2, Bax, VEGF, NF-κBp65, and β-actin were added and incubated overnight at 4 °C. After TBST buffer rinsing, the PVDF membrane was incubated with goat anti-rabbit secondary antibody (1:10,000) at room temperature for 2 h. After TBST buffer rinsing, the membrane was treated with ECL luminescent solution. Finally, the gel image analysis system is used to take photos and determine the optical density of protein bands, and the relative grayscale values of each protein band are calculated using β-actin as internal parameter.

2.12. Autophagy Assay

After digestion, 1×10^5 cells were cultured in a 24-well plate in which a cover glass was placed overnight. MCF-7 cells were exposed to various concentrations of SNH (0, 100,

200, and 250 μg/mL) for 48 h and then washed in PBS three times. The steps of cellular immunofluorescence staining were as described previously [51]. A total of 500 μL of 4% polyformaldehyde was added to fix cells for 20 min; then, 0.1% Triton X-100 was applied for 20 min after PBS washing. Goat serum working solution was added for blocking to avoid non-specific adsorption for 20 min and removed; 2 mL of LC-3 primary antibody (1:300) was added and the samples were incubated in the 4 °C fridge all night. The next day, cells were rinsed with PBS 3 times, and diluted goat anti rabbit fluorescent secondary antibody (1:500) was added to incubate at 37 °C for 2 h. After rinsing with PBS 3 times, DAPI was added to counterstain for 5 min, then the cover glass was sealed and observed under inverted fluorescence microscope (Nikon C2+).

2.13. Acute Toxicity Test of SNH

This experiment was conducted in accordance with the previous protocol [52]. Different concentrations of SNH solution were prepared with K-Medium solution, and eight groups were designed: 0, 25, 50, 100, 200, 300, 400, and 500 μg/mL. A total of 500 μL of solution of each group was added to the 24-well plate. Each concentration group was set up with 3 multiple-plate wells and seeded in 10 ± 1 nematodes synchronized in the L4 stage. After exposure for 48 h, the number of survivals and deaths of *C. elegans* was observed under a somatotype microscope. The mortality rate of *C. elegans* in each concentration was calculated.

2.14. Statistical Analysis

All experiments should be repeated at least 3 times. The values are represented as the mean ± standard deviation. All data were analyzed and plotted using Graghpad przsm 7.0 software. Significance is shown as $p \leq 0.05$ (*), $p \leq 0.01$ (**), or $p \leq 0.001$ (***).

3. Results

3.1. Molecular Property of SNH

The structure of SNH is displayed in Figure 1, and its molecular properties include molecular weight: 330.41; Octanol/Water Partition Coefficient: 2.66; total polar surface area: 91.9; calculation of hydrophobic parameters: 4.62; number of hydrogen bond receptors: 0; number of hydrogen bond donors: 5; and a certain degree of irritation and mutagenicity. The molecule was evaluated according to four rule parameters simplified by Lipinski [53], which included no more than 5 hydrogen bond donors, no more than 10 hydrogen bond receptors, no more than 5 octanol/water partition coefficients, and a molecular weight below 500. Thus, SNH did not violate this rule and was proved to be an effective drug candidate.

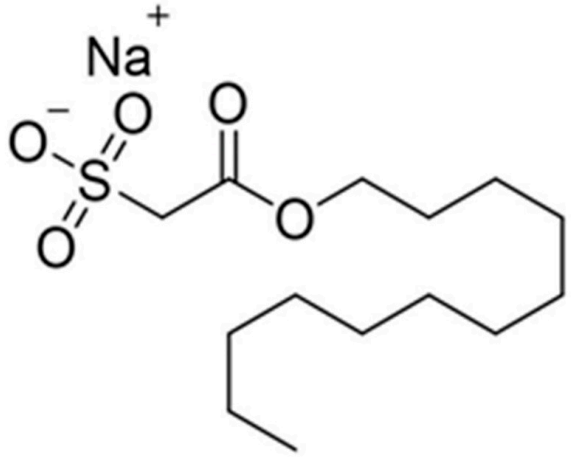

Figure 1. The structure of SNH.

3.2. Docking Analysis of SNH at the EGFR-TK

As SNH obeys Lipinski's rule for its drug (i.e., its molecular nature), docking analysis with EGFR-TK protein domain was carried out, and the results are displayed in Table 2. The shape complementarity was observed between SNH and the binding pocket in Figure 2 which suggested that SNH exhibited a good binding ability with respect to the target protein. The three conformations were finally selected as the most potent EGFR-TK inhibitor of SNH based on its least binding energy, -CDOCKER energy, and binding modes. The different significant chemical interactions, salt bridge, alkyl, hydrogen bonds, and so on, have been presented in the following figures. As shown in Figure 2a, conformation 1 was well matched to the EGFR-TK model and formed a hydrogen bond interaction with the Cys773, Asp776, and Tyr777. Simultaneously, residues Lys721 generated hydrophobic interactions with SNH, which had the same result as the crystalline composites of the original. As presented in Figure 2b, conformation 2 was found to fully embed into the active pocket, and it interacted with amino acids Lys692, Lys704, and Met769 via H-bonds. Meanwhile, Arg817 interacted with alkyl via the hydrophobic bond and generated salt bridge with Lys692, which had a great effect on the stability of the ligand-protein structure. In addition, the conformation 3 formed an attractive charge with Lys721 and generated hydrogen bond interactions with Thr830, Thr766, and Asp831 in Figure 2c. It is well known that hydrogen bonds are essential for binding affinity and interaction between small molecules and proteins. Therefore, the method demonstrated the accuracy and reliability of the docking, and subsequent experimental results will confirm the EGFR-TK-inhibitory effect of SNH as determined by molecular docking experiments.

Table 2. Grading and interacting residues of the compounds against the EGFR-TK domain.

SNH Conformation	Binging Energy	-CDOCKER Energy	Hydrogen Bond	Hydrophobic	Attractive Charge	Salt Bridge
1	−26.142	37.1847	Cys773, Asp776, Tyr777	Lys721	-	-
2	−42.8495	36.2745	Lys692, Lys704, Met769	Arg817	-	Lys692
3	−49.6815	34.4638	Thr830, Thr766, Asp831	-	Lys721	-

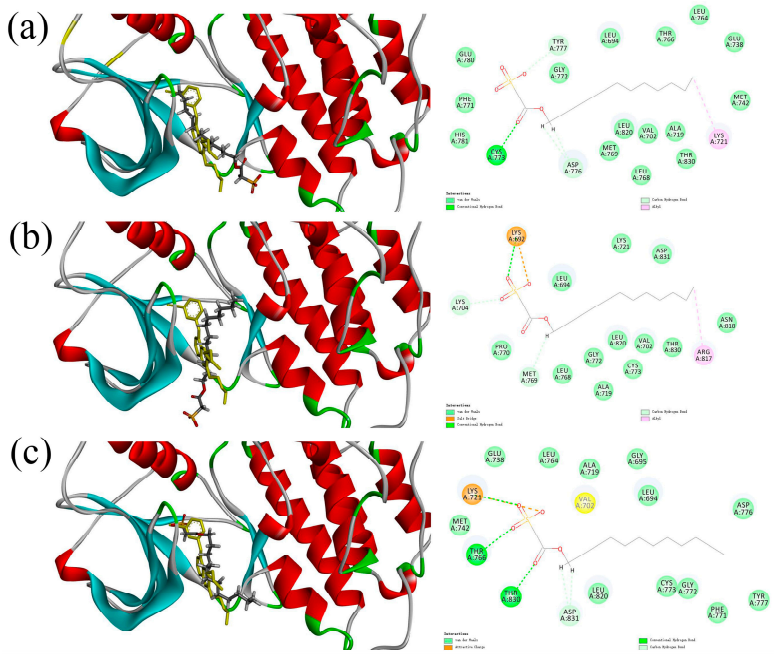

Figure 2. Alignment of the docked SNH with 4-annilinoquinazoline in the crystallographic complex. SNH and 4-annilinoquinazoline in the crystallographic complex are brown and yellow, respectively. The receptor–ligand interaction of SNH with the EGFR-TK active site: (**a**) conformation 1; (**b**) conformation 2; (**c**) conformation 3.

3.3. Cytotoxicity Assay

The cytotoxic influence of SNH on the proliferation of human breast cancer MCF-7 cells and human cervical carcinoma Hela cells is analyzed using an MTT experiment. As seen in Figure 3, SNH significantly suppressed the proliferative capacity of MCF-7 and Hela cells and appeared to be a dose dependent. Moreover, MFC-7 cells seemed to be more sensitive to SNH than Hela cells, and the inhibition rate was up to 70% in the 250 μg/mL SNH treated group. These results threw light on the fact that SNH has an obvious cytotoxic effect on both cell lines and has a broad spectrum of anticancer properties.

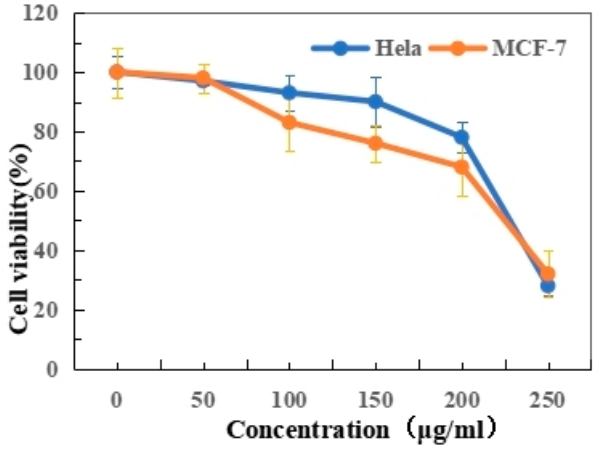

Figure 3. SNH inhibited the proliferation of MCF-7 and Hela cells. MCF-7 and Hela cells were incubated with different concentrations of SNH (0, 50,100, 150, 200, and 250 μg/mL), respectively, for 48 h. Then, cell proliferation of samples was analyzed by MTT assay. Data are presented as mean ± SD of five parallel wells from three independent experiments.

3.4. SNH Decreased the Clonogenesis of MCF-7 Cells

The ability of individual cells to form clones might indirectly reflect the proliferation ability of cells; therefore, the influence of different concentrations of SNH on the colony-forming ability of MCF-7 cells was detected. As displayed in Figure 4, accompanied by an increasing concentration of SNH, the number of clones formed in MCF-7 cells gradually reduced by 70% and the size of the colonies formed also decreased significantly compared with the control group. Moreover, the number of cell clones formed in the 200 μg/mL and 250 μg/mL SNH-treated groups were 129.53 and 140.61, respectively, and showed significant differences compared to the control group (472.68), but there was no statistical difference between these two SNH-treated groups. Moreover, the size of cell clones in the 200 μg/mL group is larger than that of those in the 250 μg/mL group. To summarize, the results demonstrated that SNH markedly reduced soft agar clonogenesis in MCF-7 cells at all concentrations, which was consistent with its cytotoxicity.

3.5. SNH Promoted the Apoptosis of MCF-7 Cells

To determine the influence of SNH on the apoptosis of MCF-7 cells, cells managed with different densities of SNH for 48 h were doubly stained using Annexin V antibody and propidium iodide (PI). Then, the quantity of apoptotic cells was checked by flow cytometry. As displayed in Figure 5A, compared with the control group, the number of apoptotic cells (including early and late apoptotic cells) was obviously promoted. In Figure 5B, cell apoptosis rates were 14.3%, 31.1%, and 44.1% in the SNH-treated groups (containing 100 μg/mL, 200 μg/mL, and 250 μg/mL), respectively. These results indicated that SNH increased the apoptotic rate of MCF-7 cells in a certain dose-dependent pattern, suggesting that SNH might play a role in the cytotoxicity on MCF-7 cells attributed to cell apoptosis.

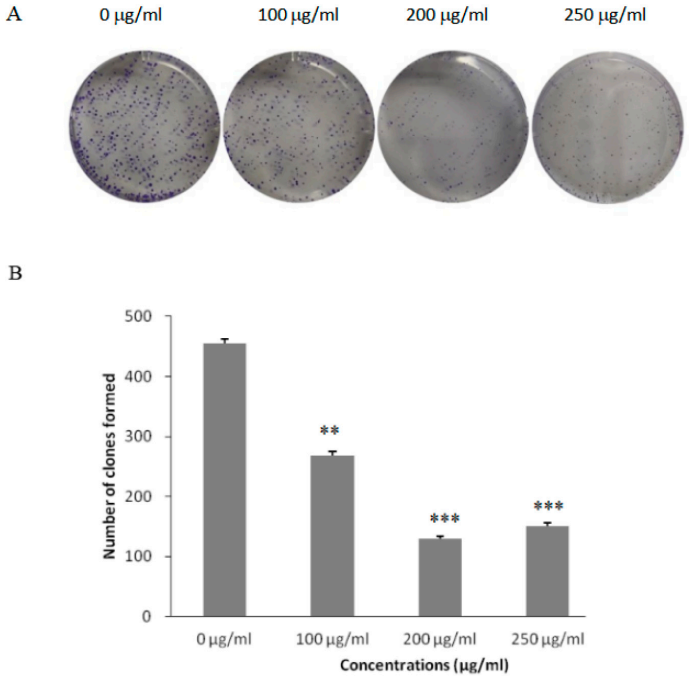

Figure 4. SNH significantly decreased the number of cell clones. MCF-7 cells were seeded in six-well plates, and each group was plated in three duplicate wells. The cells were exposed to different density of SNH (0, 100, 200, and 250 μg/mL), respectively, at 37 °C for 48 h. Then, the culture medium containing SNH was changed and cells continued to be cultured for 10 d. The colonies were treated with 4% paraformaldehyde for 30 min and then stained using 0.5% crystal violet solution for 20 min. (**A**) The colonies were observed by light microscopy. (**B**) The amount of cell clones was analyzed by Image J. ** $p < 0.01$; *** $p < 0.001$ versus the control group.

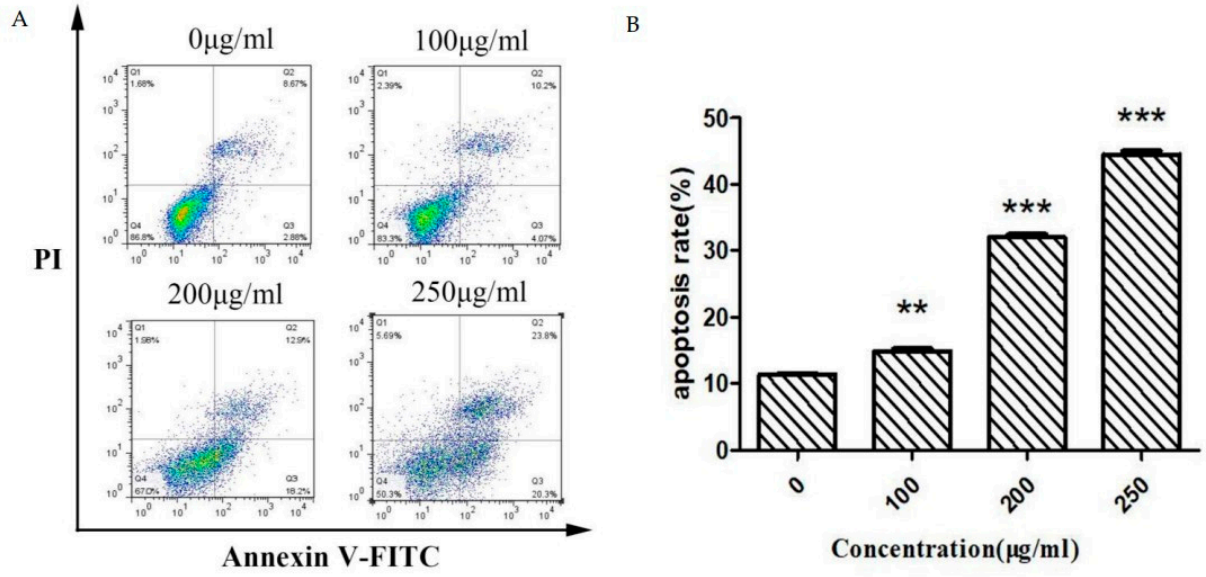

Figure 5. SNH promoted the apoptosis of MCF-7 cells by Annexin-V and PI staining. (**A**) Dot plots of Annexin V/PI staining ware displayed. (**B**) The percentages of apoptotic cells with SNH treatment were plotted. The data are from three independent experiments. ** $p < 0.01$; *** $p < 0.001$ versus the control group.

3.6. Hoechst Staining

MCF-7 cells were treated with Hoechst33258 staining in order—judging from cell morphology—to further validate whether SNH urged the apoptosis of MCF-7 cells. When

MCF-7 cells were dealt different densities of SNH for 48 h, the quantity of adherent cells notably decreased, and there appeared to be a certain dose dependence. The apoptotic cells emerged bright blue and had shrunk nuclei. In Figure 6, some cells in the 100 μg/mL group were shown to be round and wrinkled. Moreover, some vesicles and apoptotic bodies appeared in the 200 μg/mL and 250 μg/mL groups, and these are the characteristics of apoptotic cells. In addition, the number of cells with apoptotic bodies was not as many as those detected by Annexin-V and PI double staining, possibly due to the fact that most apoptotic cells did not adhere to the wall and are not stained and counted.

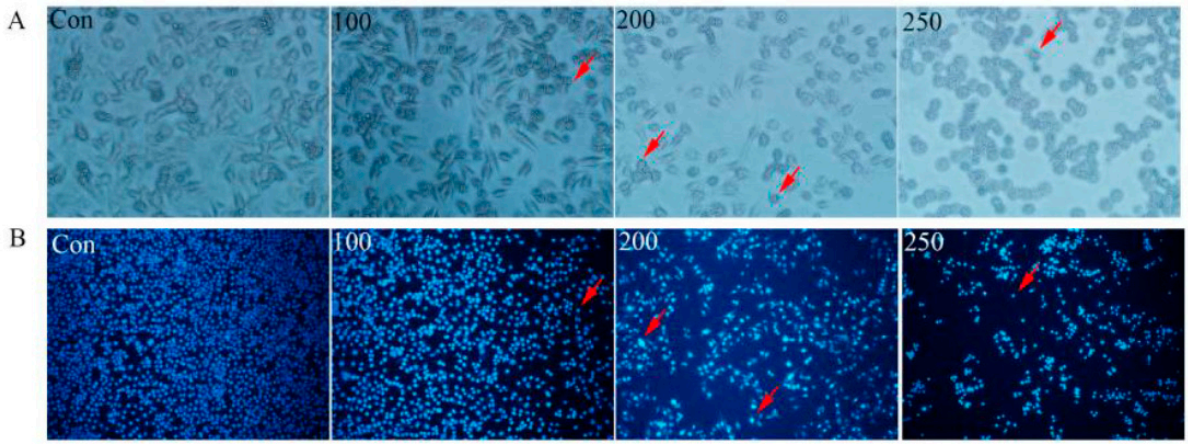

Figure 6. SNH induced the apoptosis of MCF-7 cells. MCF-7 cells were dealt with SNH (0, 100, 200, and 250 μg/mL) for 48 h. (**A**) Morphology of MCF-7 cells examined under a phase contrast microscope (200× magnification). (**B**) The nuclear morphology of MCF-7 cells analyzed via Hoechst33258 staining (100× magnification). The red arrow points to apoptotic cells.

3.7. Wound Healing Analysis

Given that cell migration is a significant cause of breast cancer metastasis and the death of patients, the effect of SNH on the migration of breast cancer cells was checked through a wound healing model in vitro. The degree of wound healing was judged by the average reduction in distance between the edges of the wounds at a series of time points in the absence or presence of SNH (0, 50, 100, 150, 200, and 250 μg/mL) stimulation. Just as displayed in Figure 7, the results revealed that MCF-7 cells in the control group had the ability to heal the wounds completely after 48 h. In particular, in the density of 250 mg/mL group, the relative healed distances were changed from 100% to 96.24%, 88.46%, 82.71%, 83.64%, 84.68%, and 81.31% at 0 h, 6 h, 12 h, 24 h, 30 h, 36 h, and 48 h, respectively. However, in the control group, the relative healed distances were 100%, 74.23%, 52.57%, 37.83%, 36.55%, 19.64, and 5.27% at different time points. These data indicated that SNH significantly reduced the migration ability of MCF-7 cells.

3.8. Relative Gene Expression Analysis

As previous studies show, the Bcl-2 family, including Bcl-2 and Bax, is considered to be an important participant in cell apoptosis via the mitochondrial pathway. NF-kB plays a major part in the proliferation and migration of cancer cells by regulating the expression of transcription factors. VEGF becomes involved in the neovascularization, tumor development, and migration of cancer cells, and its notable decline is considered as an important sign of the antitumor effect. In order to intensively explore the mechanism by which SNH influenced the apoptosis and migration of MCF-7 cells, the levels of Bcl-2, Bax, VEGF, NF-κBp65, and GADPH were checked through RT-PCR. As is displayed in Figure 8A, the expression of Bax was markedly up-regulated after exposure to 250 μg/mL of SNH compared with the untreated group, while the expressions of Bcl-2 decreased by increasing SNH concentration. In a word, the ratio of Bax and bcl-2 elevated significantly, which would result in cell apoptosis induced by SNH. In addition, SNH decreased the levels of

VEGF in MCF-7 cells, which further supported the results of SNH inhibiting the migration of MCF-7 cells. The expression of NF-κBp65 did not seem to be obvious in Figure 8A. Furthermore, relative gene expressions in the protein level were also analyzed through western blotting. In Figure 8B, excepting Bax, SNH notably decreased the expressions of Bcl-2, VEGF, and NF-κBp65. In general, these are consistent with PCR. However, there are some slight differences of gene expression quantity in mRNA and protein levels—especially for NF-κBp65, which may be related to the regulation of translation level.

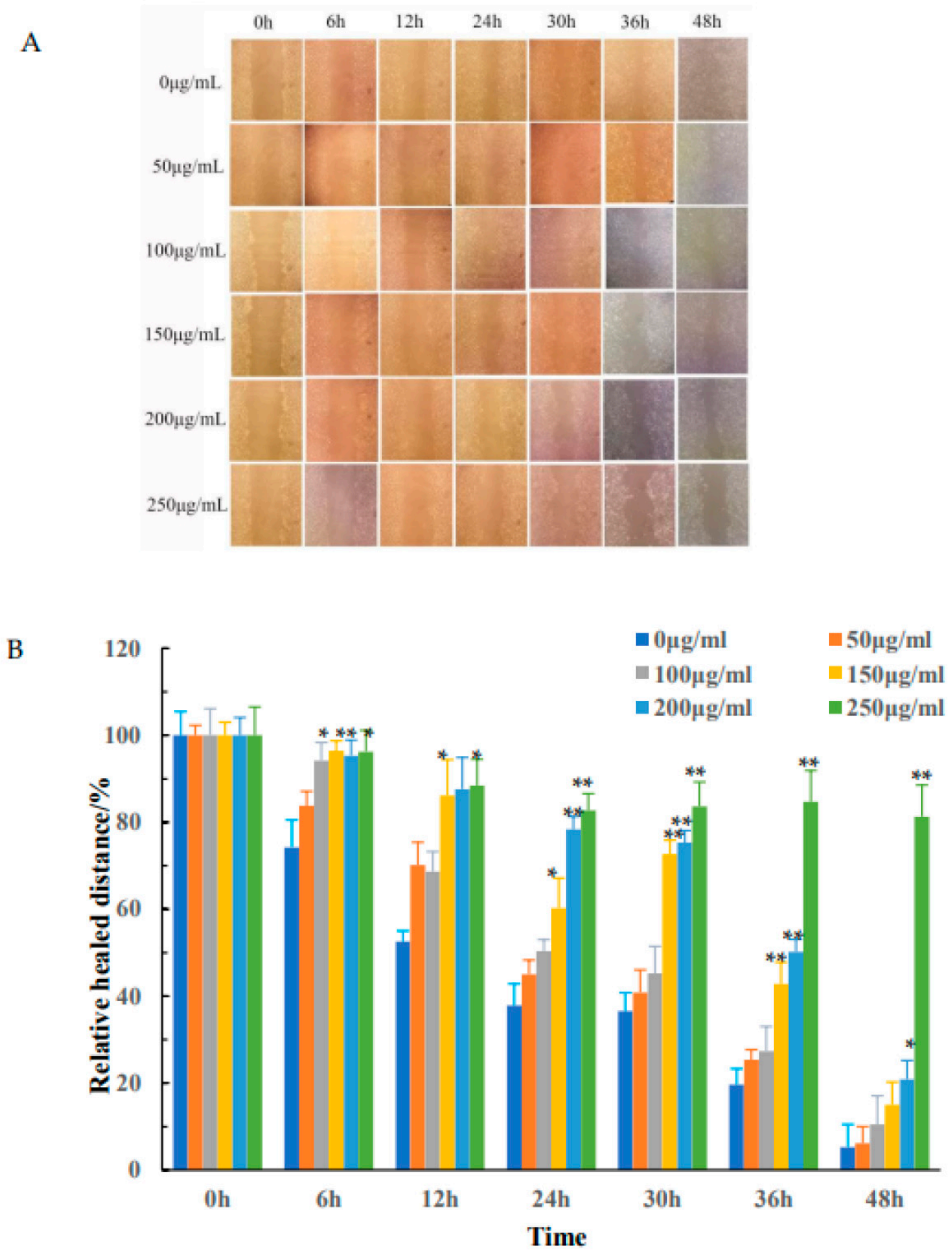

Figure 7. SNH inhibit MCF-7 cells' migration. Images (100×) exhibited that MCF-7 cells migrated into wounded area in an in vitro scratch wound healing test. After MCF-7 cells were exposed to various density of SNH (0, 50, 100,150, 200, nd 250 μg/mL) for 48 h, images were photographed at 6 h, 12 h, 24 h, 30 h, 36 h, and 48 h. (**A**) shows cells photographed under a microscope, and (**B**) is the statistical graph of the crawling distances of MCF-7 cells. This assay was performed in triplicate. * $p < 0.05$; ** $p < 0.01$ versus the control group.

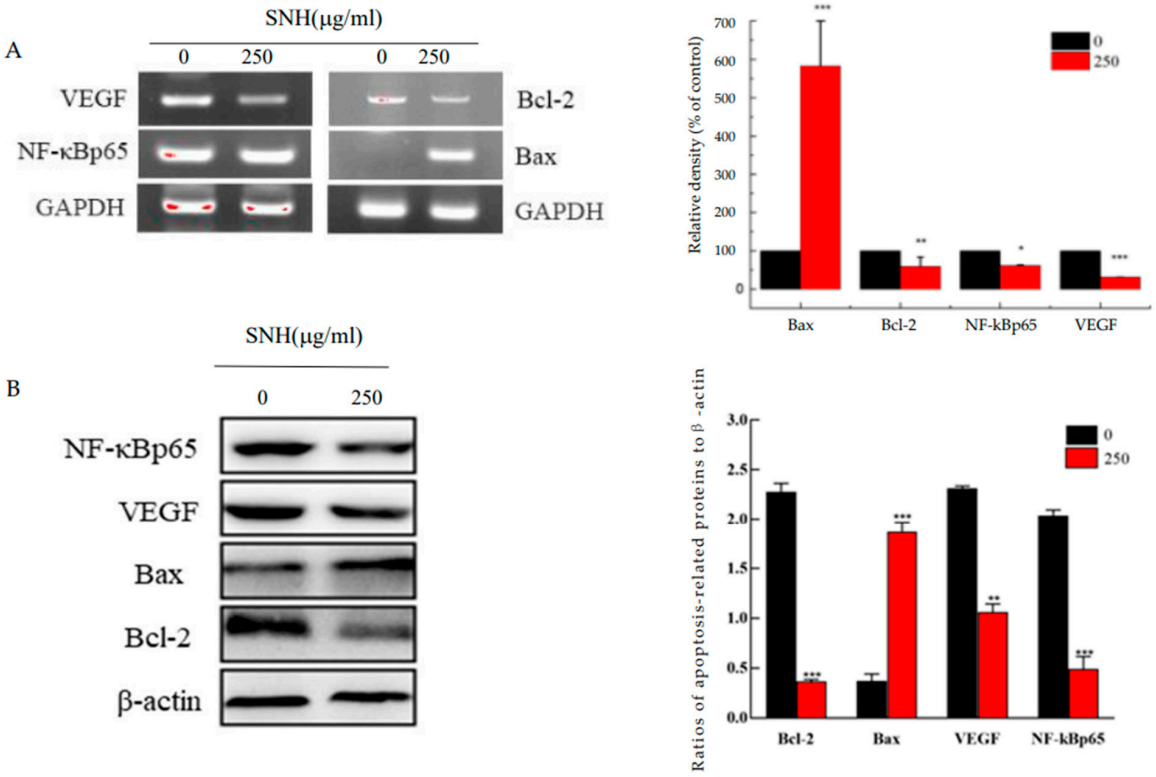

Figure 8. SNH regulated the expressions of Bcl-2, Bax, NF-kBp65, and VEGF in MCF-7 cells. After cells were cultured with SNH (250 μg/mL) for 48 h, the expressions of Bcl-2, Bax, NF-kBp65, and VEGF were analyzed by RT-PCR and western blotting. GADPH and β-actin were used as internal parameters for comparison with other genes. (**A**,**B**) represent the results of RT-PCR and western blotting, respectively. The data represent three independent experiments. * $p < 0.05$; ** $p < 0.01$; *** $p < 0.01$ versus the control group.

3.9. Autophagy Assay

Autophagy is an important pathway to maintain cellular homeostasis via removing dysfunctional proteins or aged organelles, and the appearance of autophagy is closely related to the decreased tumor growth. To probe if the cell death is related to cell autophagy, LC3, an autophagy marker, was detected by fluorescence microscope. As shown in Figure 9, MCF-7 cells were checked under an inverted fluorescence microscope after LC3/DAPI double staining, and obvious autophagosomes were found. Compared to the control group, dots of small green fluorescence were observed in the middle and high dose group, and the green, fluorescent spots were autophagosomes containing LC3. Moreover, accompanied by an increase in SNH concentration, the incidences of spot-like green fluorescence in the cells increased.

3.10. Toxicity to C. elegans

C. elegans, a multicellular organism, is extensively regarded as a model organism in the field of basic biology and medical science. It has been used as an ideal living animal model for screening anticancer drugs. In this study, *C. elegans* was used to simulate parasites to test the potential antiparasitic effect of SNH which might partly reflect its antitumor effect. After the nematodes were exposed to SNH for 48 h, the bodies of the dead nematodes were transparent and stiff, and SNH decreased the motor ability, the movement frequency, and the amplitude of the surviving *C. elegans* (Table 3). Furthermore, the higher the SNH concentration, the higher the mortality rate of *C. elegans*. The median lethal concentration (LD50) of SNH was 40.46 μg/mL.

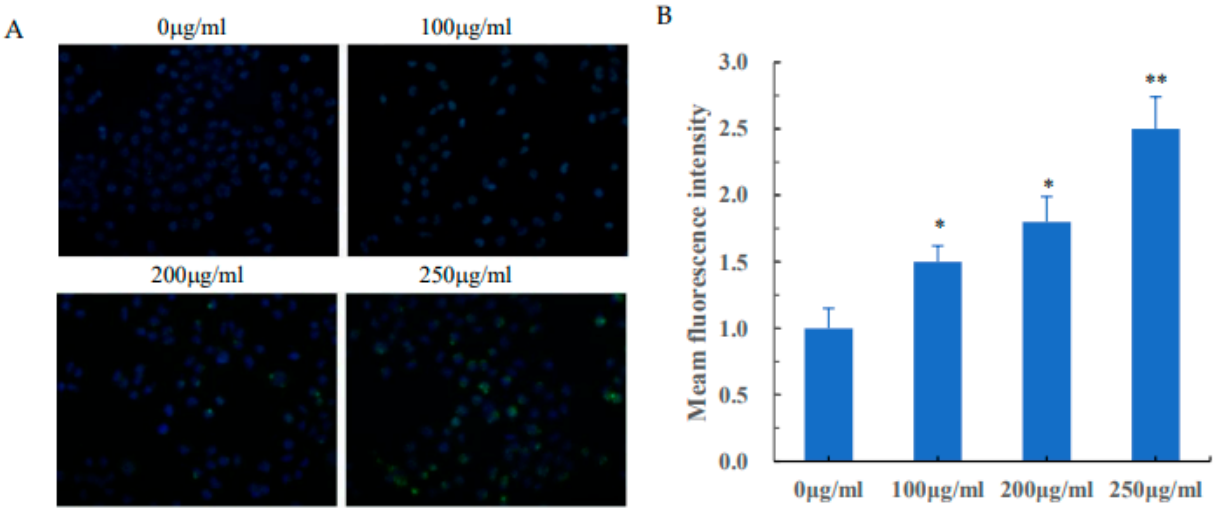

Figure 9. SNH induced the autophagy of MCF-7 cells. After cells were exposed to various dosages of SNH (0, 100, 200, and 250 μg/mL) for 48 h, they were subsequently stained with primary LC3 antibody and FITC labeled secondary antibody and counterstained by DAPI solution. Cells were observed using a fluorescence microscope. (**A**) Representative immunofluorescence staining images of LC3 in each group. (**B**) Analysis of LC3 mean fluorescence intensity of each group. This experiment was performed three times. * $p < 0.05$; ** $p < 0.01$ versus the control group.

Table 3. Effects of various concentrations of SNH for 48 h on the mortality of *C. elegans*.

Group	Drug Concentration (μg/mL)	Logarithmic Concentration (μg/mL)	Total Number of Nematodes (Strips)	Number of Deaths (Articles)	Death Rate	LC50 (μg/mL)	95% Confidence Interval (μg/mL)
1	500	2.699	10	10	100%	40.46	22.84–58.84
2	400	2.602	10	10	100%		
3	300	2.407	10	10	100%		
4	200	2.301	10	9	90%		
5	100	2.000	10	9	90%		
6	50	1.699	10	7	70%		
7	25	1.398	10	2	20%		
8	0	0.000	10	0	0%		

4. Discussion

In China, *Houttuynia*, as a plant with medicinal and edible homology, has been popularly adopted in the clinical treatment of microbial virus infections and inflammation for many years. Some of its components exhibit various impressive effects, such as its flavonoids in lung protection [54], the ethyl acetate extract in decreasing live damage [55], 2-undecanone and polysaccharides in anti-lung cancer [56,57], and so on. The numerous functions of *Houttuynia* are closely related to its anti-inflammatory effects. Previous studies have reported its anti-inflammatory mechanism; *Houttuynia* plays roles in increasing c-Fos expression at the protein level in macrophages [58], inhibiting a cytokine pathway mediated by NF-kB, and regulating relative protein expressions of the MAPK signaling pathway in endometrial epithelial cells [59,60].

SNH, a volatile oil extracted from *Houttuynia*, might play its biological role through binding to a special cell membrane protein. EGFR, the expression product of the proto-oncogene c-erbB1 [61], is widely distributed on many malignant epithelial cells, especially breast cancer cells [62]. A lot of studies showed that EGFR is excessively expressed in patients with triple-negative breast cancer [63,64], and molecules related to the EGFR signaling pathway promoted the expression of the S100 gene in HER2-positive breast tissue [65]. Stamos [39] previously reported that 4-annilinoquinazoline interact with EGFR as a potent EGFR inhibitor, performing the analysis with DS Software. Moreover, the results of docking discovered that six amino acids (Leu694, Met769, Lys721, Gln767, Thr766,

and Leu764) situated in the binding pocket of EGFR had a crucial role in its binding to compounds. Therefore, EGFR also entered the range of membrane surface proteins that we selected for SNH binding. In addition, as shown in Table 2, SNH displayed a considerable drug score. Consequently, SNH molecules were explored for docking with EGFR-TK. The interaction results showed (see Figure 2) that SNH molecules were able to interact with these residues mentioned above, and they showed similar inhibitory activity on EGFR-TK to 4-annilinoquinazoline. Thus, SNH may have the potential to be a candidate in the treatment of breast cancer in clinics through inhibiting EGFR-TK.

The biological influence of SNH on MCF-7 cells was not only simulated by DS software but was also examined in vitro. Our results showed that SNH decreased the proliferative capacity of MCF-7 cells via an apoptotic pattern and suppressed cell migration. In previous studies, polysaccharides in *Houttuynia* restrained the proliferation of human lung cancer A549 cells by means of cell apoptosis and arresting cell cycle [57]. Quercetin, one of the most important flavonoids in HCT, repressed human melanoma cells growth by promoting programmed cell death [66]. *Houttuynia* suppressed the proliferation of breast cancer cells, MDA-MB-468, [67] and the migration of human mast cells, HMC-1 [68]. Results in our studies were in good concordance with the above studies in demonstrating that SNH displayed similar antiproliferative, proapoptotic, and migration inhibitory characteristics to polysaccharides and quercetin in *Houttuynia*.

In this study, the level of some genes related to cell proliferation, apoptosis, and migration was also detected in order to discover the potential mechanism underpinning the influence of SNH on breast cancer cells. Bax and Bcl-2 are two crucial protein members of the Bcl-2 family, which are proapoptotic and antiapoptotic, and their ratio determines whether a cell's fate tends towards apoptosis or survival [69]. Moreover, VEGF participates not only in tumor growth but also in tumorigenesis. NF-kBp65 is involved in regulating many biological processes, such as humoral and cellular immune responses, inflammatory reactions, cell apoptosis, and tumor formation [70,71]. Our results discovered that SNH increased the level of Bax and down-regulated the expressions of Bcl-2, VEGF, and NF-kBp65. Kim [72] even found that HCT disrupted the protein expressions of the Bcl-2 family (Bax, Bcl-2, and Bcl-XL) and activated hypoxia-inducible factor (HIF)-1A-Forkhead box (FOX)O3 and myocyte enhancer factor 2A (MEF2A) pathways to promote the apoptosis of HepG2 cells. In addition, Prommaban discovered that HCT decreased the level of Bcl-XL while increasing expressions of Smac/Diablo, Bax and glucose-regulated protein 78, which resulted in the apoptosis of human leukemic molt-4 cells [73]. Furthermore, HC appeared to inhibit NF-κB expression [59], and Oxymatrine inhibited the proliferation and migration of lung cancer cells by down-regulating the level of VEGF [74]. Our results displayed that SNH might regulate the apoptosis and proliferation of MCF-7 cells by suppressing the expression of NF-kBp65 and enhancing the proportion of Bax and Bcl-2, and it weakened cell migration capacity partly through reducing the expression of VEGF.

Autophagy is an important process in eukaryotic organisms which is evolutionarily conserved in the turnover of intracellular substances. It plays a critical role in keeping cellular homeostasis during extreme conditions such as hypoxia, heat stress, and the accumulation of reactive oxygen. However, abnormal autophagy leads to various diseases, including Alzheimer's disease, cancer, and microorganism infection [75]. Autophagy plays a bidirectional role by inhibiting tumor initiation but supporting tumor progression [76], and its mechanisms have not been fully studied. Aita reported that in 40~70% patients suffering from breast cancer, prostate cancer, and ovarian cancer, the single allele gene of Beclin that can induce autophagy vesicle formation was missing [77]. For example, in MCF-7 cells, Beclin was not detected at the protein level [78]. Yue also discovered that there was decreased autophagy and increased tumor incidence in Beclin single-allele knockout mice with respect to ovarian cancer, lung cancer, liver cancer, and lymphatic cancer [79]. These findings further confirmed the relationship between autophagy and cancer and suggested that autophagy might become a target for cancer inhibition and treatment. Our results revealed that a high dose of SNH significantly induced the appearance of autophagosomes,

which might also induce MCF-7 cell apoptosis in the next stage. Wang [80] revealed that autophagy was involved in flavopiridol-induced MCF-7 cell death, and autophagy inhibition enhanced the tumor cell survivability, and our results are consistent with these findings. Moreover, EGFR is a receptor with tyrosine kinase activity, and its expression is enhanced in many solid tumors. It phosphorylates Beclin1 and promotes its homodimerization. The latter's binding with Rubicon reduces the formation of the PI3KC3-C1 complex with autophagy activity, which ultimately leads to autophagy inhibition and tumor growth [81]. According to our results of molecular docking, SNH might act as an inhibitor of ERFR-TK, promote autophagy via inhibiting Beclin 1 phosphorylation, and induce the apoptosis of MFC-7 cells. These, in turn, confirm the results of molecular simulations using DS software.

The epidermal growth factor receptor (EGFR) is involved in the development of cancer, including tumor occurrence, invasion, metastasis, and angiogenesis [82], and is recognized as a cancer treatment target. EGFR tyrosine kinase (TK) inhibitors, such as gefitib [83], have been developed as anticancer drugs. Mansour [84] reported that a new EGFR-TK inhibitor had previously promoted the apoptosis of HepG-2, HCT-116, MCF-7, Hep2, PC3, and Hela cells. El-Gazzar [85] also showed that new quinazolinone-based derivatives presented significant anticancer activity. At present, due to their simple structure, short growth cycle, high homology between genes and human genes, easy cultivation, suitability for high-throughput screening, and, especially, their possessing the EGFR homologous LET-23, *C. elegans* are widely used not only in drug preliminary toxicity evaluation but also in screening antitumor drugs in vivo [41]. Markowicz reported that *a*-mangostin extracted from the skin of mangosteen not only had antitumor effects on squamous carcinoma and glioblastoma multiforme through the promotion of cell apoptosis but also has antinematode effects [86]. In this study, SNH had a significant antinematode effect, just like a well-known anthelmintic mebendazole had an apparent antitumor effect [41]. Therefore, the antiparasitic effect of SNH might partly reflect its potential antitumor effect in vivo.

5. Conclusions

In summary, SNH markedly inhibited the migration and proliferation ability of MCF-7 cells, stimulated cell apoptosis by elevating the ratio of apoptotic and antiapoptotic proteins, induced cell autophagy, and played a notable antiparasitic role. These all indicated that SNH was a very promising candidate drug for the therapy of breast cancer. Interestingly, SNH not only demonstrated antitumor activity, but also antinematode activity, the mechanism of which needs to be explored in depth in the future.

Author Contributions: L.Y. and Y.H. planned and designed the research work together. J.X., M.S., Y.L. and Z.G. assisted in the laboratory work. J.Z. reviewed the manuscript. All authors have read and agreed to the published version of the manuscript.

Funding: This research received no external funding.

Institutional Review Board Statement: Not applicable.

Informed Consent Statement: Not applicable.

Data Availability Statement: The data achieved through experiments in this article can be obtained via the corresponding authors.

Acknowledgments: We express thanks to Ren Jie for kindly providing MCF-7 and Hela cells and Ziheng Zhuang for providing *E. coli* OP50 and *C. elegans*.

Conflicts of Interest: The authors declare no conflict of interest.

References

1. Sung, H.; Ferlay, J.; Siegel, R.L.; Laversanne, M.; Soerjomataram, I.; Jemal, A.; Bray, F. Global cancer statistics 2020: GLOBOCAN estimates of incidence and mortality worldwide for 36 cancers in 185 countries. *CA Cancer J. Clin.* **2021**, *71*, 209–249. [CrossRef] [PubMed]
2. Fidler, M.M.; Soerjomataram, I.; Bray, F. A global view on cancer incidence and national levels of the human development index. *Int. J. Cancer* **2016**, *139*, 2436–2446. [CrossRef]

3. Peairs, K.S.; Choi, Y.; Stewart, R.W.; Sateia, H.F. Screening for breast cancer. *Semin. Oncol.* **2017**, *44*, 160–172. [CrossRef] [PubMed]
4. Liu, K.; Zhang, W.N.; Dai, Z.M.; Wang, M.; Tian, T.; Liu, X.H.; Kang, H.F.; Guan, H.T.; Zhang, S.Q.; Dai, Z.J. Association between body mass index and breast cancer risk: Evidence based on a dose-response meta-analysis. *Cancer Manag. Res.* **2018**, *10*, 143–151. [CrossRef] [PubMed]
5. Hulka, B.S.; Moorman, P.G. Breast cancer: Hormones and other risk factors. *Maturitas* **2008**, *61*, 203–213. [CrossRef]
6. Martin, A.M.; Weber, B.L. Genetic and hormonal risk factors in breast cancer. *J. Natl. Cancer Inst.* **2000**, *92*, 1126–1135. [CrossRef]
7. Carneiro, B.A.; El-Deiry, W.S. Targeting apoptosis in cancer therapy. *Nat. Rev. Clin. Oncol.* **2020**, *17*, 395–417. [CrossRef]
8. Singh, R.; Letai, A.; Sarosiek, K. Regulation of apoptosis in health and disease: The balancing act of BCL-2 family proteins. *Nat. Rev. Mol. Cell Biol.* **2019**, *20*, 175–193. [CrossRef]
9. Bieging, K.T.; Mello, S.S.; Attardi, L.D. Unravelling mechanisms of p53 mediated tumour suppression. *Nat. Rev.* **2014**, *14*, 359–370. [CrossRef]
10. Yu, X.L.; Liu, Y.Q.; Wang, Y.Z.; Mao, X.G.; Zhang, Y.J.; Xia, J.Y. Baicalein induces cervical cancer apoptosis through the NF-κB signaling pathway. *Mol. Med. Rep.* **2018**, *17*, 5088–5094. [CrossRef]
11. Schwartz, C.; Willebrand, R.; Huber, S.; Rupec, R.A.; Wu, D.; Locksley, R.; Voehringer, D. Eosinophil-specific deletion of IκBα in mice reveals a critical role of NF-κB-induced Bcl-xL for inhibition of apoptosis. *Blood* **2015**, *125*, 3896–3904. [CrossRef] [PubMed]
12. Concetti, J.; Wilson, C.L. NFκB1 and Cancer: Friend or Foe? *Cells* **2018**, *7*, 133. [CrossRef] [PubMed]
13. Cao, W.Y.; Li, J.H.; Yang, K.P.; Cao, D.L. An overview of autophagy: Mechanism, regulation and research progress. *Bull. Cancer* **2021**, *108*, 304–322. [CrossRef] [PubMed]
14. Piffoux, M.; Eriau, E.; Cassier, P.A. Autophagy as a therapeutic target in pancreatic cancer. *Br. J. Cancer* **2021**, *124*, 333–344. [CrossRef]
15. Lu, Z.Y.; Cheng, M.H.; Yu, C.Y.; Lin, Y.S.; Yeh, T.M.; Chen, C.L.; Chen, C.C.; Wan, S.W.; Chang, C.P. Dengue nonstructural protein 1 maintains autophagy through retarding caspase-mediated cleavage of beclin-1. *Int. J. Mol. Sci.* **2020**, *21*, 9702–9721. [CrossRef]
16. Monastyrska, I.; Klionsky, D.J. Autophagy in organelle homeostasis: Peroxisome turnover. *Mol. Aspects Med.* **2006**, *27*, 483–494. [CrossRef]
17. Das, S.; Shukla, N.; Singh, S.S.; Kushwaha, S.; Shrivastava, R. Mechanism of interaction between autophagy and apoptosis in cancer. *Apoptosis* **2021**, *26*, 512–533. [CrossRef]
18. Smith, B.D.; Bellon, J.R.; Blitzblau, R.; Freedman, G.; Haffty, B.; Hahn, C.; Halberg, F.; Hoffman, K.; Horst, K.; Moran, J.; et al. Radiation therapy for the whole breast: Executive summary of an American Society for Radiation Oncology (ASTRO) evidence-based guideline. *Pract. Radiat. Oncol.* **2018**, *8*, 145–152. [CrossRef]
19. Burstein, H.J.; Lacchetti, C.; Anderson, H.; Buchholz, T.A.; Davidson, N.E.; Gelmon, K.E.; Giordano, S.H.; Hudis, C.A.; Solky, A.J.; Stearns, V.; et al. Adjuvant endocrine therapy for women with hormone receptor–positive breast cancer: American Society of Clinical Oncology clinical practice guideline update on ovarian suppression. *J. Clin. Oncol.* **2016**, *34*, 1689–1701. [CrossRef]
20. Kang, D.; Kim, I.R.; Choi, E.; Im, Y.H.; Park, Y.H.; Ahn, J.S.; Lee, J.E.; Nam, S.J.; Lee, H.K.; Park, J.H.; et al. Permanent chemotherapy-induced alopecia in patients with breast cancer: A 3-year prospective cohort study. *Oncologist* **2019**, *24*, 414–420. [CrossRef]
21. Li, L.; Zhu, X.; Yang, Y.; He, J.; Yi, J.; Wang, Y.; Zhang, J. Cognitive emotion regulation: Characteristics and effect on quality of life in women with breast cancer. *Health Qual. Life Outcomes* **2015**, *13*, 51. [CrossRef] [PubMed]
22. Zhang, W.P.; Cai, J.X.; Chen, S.Y.; Zheng, X.W.; Hu, S.S.; Dong, J.L.; Xing, J.F.; Dong, Y.L. Paclitaxel resistance in MCF-7/PTX cells is reversed by paeonol through suppression of the SET/phosphatidylinositol 3-kinase/Akt pathway. *Mol. Med. Rep.* **2015**, *12*, 1506–1514. [CrossRef]
23. Bian, Y.; Wang, G.; Zhou, J.; Yin, G.; Liu, T.; Liang, L.; Yang, X.; Zhang, W.; Ni, K.; Tang, D.; et al. *Astragalus membranaceus* (Huangqi) and *Rhizoma curcumae* (Ezhu) decoction suppresses colorectal cancer via downregulation of Wnt5/β-Catenin signal. *Chin. Med.* **2022**, *17*, 11. [CrossRef] [PubMed]
24. Zhang, H.M.; Zhang, J.L.; Ding, H.; Chen, R.; Liang, F.X. Clinical value of Tongguanteng (Radix seu *Herba Marsdeniae Tenacissimae*) extract combined with chemotherapy in the treatment of advanced non-small cell lung cancer: A Meta-analysis. *J. Tradit. Chin. Med.* **2016**, *36*, 261–270.
25. Lin, W.F.; Lu, J.Y.; Cheng, B.B.; Ling, C.Q. Progress in research on the effects of traditional Chinese medicine on the tumor microenvironment. *J. Integr. Med.* **2017**, *15*, 282–287. [CrossRef] [PubMed]
26. Shen, H.S.; Wen, S.H. Effect of early use of Chinese herbal products on mortality rate in patients with lung cancer. *J. Ethnopharmacol.* **2018**, *211*, 1–8. [CrossRef] [PubMed]
27. Wu, Z.; Deng, X.Y.; Hu, Q.C.; Xiao, X.L.; Jiang, J.; Ma, X.; Wu, M.Q. *Houttuynia cordata* Thunb: An ethnopharmacological review. *Front. Pharmacol.* **2021**, *12*, 714694. [CrossRef]
28. Roe, K. An inflammation classification system using cytokine parameters. *Scand. J. Immunol.* **2021**, *93*, 6–10. [CrossRef]
29. Lee, H.J.; Seo, H.S.; Kim, G.J.; Jeon, C.Y.; Park, J.H.; Jang, B.H.; Park, S.J.; Shin, Y.C.; Ko, S.G. *Houttuynia cordata* Thunb inhibits the production of pro-inflammatory cytokines through inhibition of the NFκB signaling pathway in HMC-1 human mast cells. *Mol. Med. Rep.* **2013**, *8*, 731–736. [CrossRef]
30. Subhawa, S.; Chewonarin, T.; Banjerdpongchai, R. The effects of *Houttuynia cordata* Thunb and piper ribesioides wall extracts on breast carcinoma cell proliferation, migration, invasion and apoptosis. *Molecules* **2020**, *25*, 1196. [CrossRef]

31. Shen, Y.H.; Cheng, M.H.; Liu, X.Y.; Zhu, D.W.; Gao, J. Sodium houttuyfonate inhibits bleomycin induced pulmonary fibrosis in mice. *Front. Pharmacol.* **2021**, *12*, 596492. [CrossRef] [PubMed]
32. Liu, G.X.; Xiang, H.; Tang, X.D.; Zhang, K.Y.; Wu, X.P.; Wang, X.L.; Guo, N.; Feng, H.H.; Wang, G.M.; Liu, L.H.; et al. Transcriptional and functional analysis shows sodium houttuyfonate-mediated inhibition of autolysis in *Staphylococcus aureus*. *Molecules* **2011**, *16*, 8848–8865. [CrossRef] [PubMed]
33. Chiow, K.H.; Phoon, M.C.; Putti, T.; Tan, B.K.H.; Chow, V.T. Evaluation of antiviral activities of *Houttuynia cordata* Thunb. extract, quercetin, quercetrin and cinanserin on murine coronavirus and dengue virus infection. *Asian Pac. J. Trop. Med.* **2016**, *9*, 1–7. [CrossRef]
34. Zhang, L.; Lv, H.; Li, Y.; Dong, N.; Bi, C.; Shan, A.; Wu, Z.; Shi, B. Sodium houttuyfonate enhances the intestinal barrier and attenuates inflammation induced by *Salmonella typhimurium* through the NF-κB pathway in mice. *Int. Immunopharmacol.* **2020**, *89*, 107058. [CrossRef]
35. Yang, L.S.; Ji, W.W.; Zhong, H.; Wang, L.Y.; Zhu, X.L.; Zhu, J. Anti-tumor effect of volatile oil from *Houttuynia cordata* Thunb. on HepG2 cells and HepG2 tumor-bearing mice. *RSC Adv.* **2019**, *9*, 31517–31526. [CrossRef]
36. Mueller, K.L.; Yang, Z.Q.; Haddad, R.; Ethier, S.P.; Boerner, J. EGFR/Met association regulates EGFR TKI resistance in breast cancer. *J. Mol. Signal.* **2010**, *5*, 8. [CrossRef]
37. Ferrer-Soler, L.; Vazquez-Martin, A.; Brunet, J.; Menendez, J.A.; De Llorens, R.; Colomer, R. An update of the mechanisms of resistance to EGFR-tyrosine kinase inhibitors in breast cancer: Gefitinib (Iressa)-induced changes in the expression and nucleo-cytoplasmic trafficking of HER-ligands. *Int. J. Mol. Med.* **2007**, *20*, 3–10. [CrossRef] [PubMed]
38. Mowafy, S.; Farag, N.A.; Abouzid, K.A. Design, synthesis and in vitro anti-proliferative activity of 4, 6-quinazolinediamines as potent EGFR-TK inhibitors. *Eur. J. Med. Chem.* **2013**, *61*, 132–145. [CrossRef]
39. Stamos, J.; Sliwkowski, M.X.; Eigenbrot, C. Structure of the epidermal growth factor receptor kinase domain alone and in complex with a 4-anilinoquinazoline inhibitor. *J. Biol. Chem.* **2002**, *277*, 46265–46272. [CrossRef]
40. Freire, T.; Casaravilla, C.; Carmona, C.; Osinaga, E. Mucin-type O-glycosylation in Fasciola hepatica: Characterisation of arcinoma associated Tn and sialyl-Tn antigens and evaluation of UDP-GalNAc: Polypeptide N-acetyl galactosaminyl transferase activity. *Int. J. Parasitol.* **2003**, *33*, 47–56. [CrossRef]
41. Dorosti, Z.; Yousefi, M.; Sharafi, S.M.; Darani, H.Y. Mutual action of anticancer and antiparasitic drugs: Are there any shared targets? *Future Oncol.* **2014**, *10*, 2529–2539. [CrossRef] [PubMed]
42. Giunti, S.; Andersen, N.; Rayes, D.; Rosa, M.J.D. Drug discovery: Insights from the invertebrate *Caenorhabditis elegans*. *Pharmacol. Res. Perspec* **2021**, *9*, e00721. [CrossRef] [PubMed]
43. Bae, Y.K.; Sung, J.Y.; Kim, Y.N.; Kim, S.; Hong, K.M.; Kim, H.T.; Choi, M.S.; Kwon, J.Y.; Shim, J. An in vivo *C. elegans* model system for screening EGFR-inhibiting anti-cancer drugs. *PLoS ONE* **2012**, *7*, e42441. [CrossRef]
44. Liu, Y.; Zhi, D.; Wang, X.; Fei, D.; Zhang, Z.; Wu, Z.; Li, Y.; Chen, P.; Li, H. Kushui Rose (*R. Setate* x *R. Rugosa*) decoction exerts antitumor effects in *C. elegans* by downregulating Ras/MAPK pathway and resisting oxidative stress. *Int. J. Mol. Med.* **2018**, *42*, 1411–1417. [CrossRef] [PubMed]
45. Sánchez-Blanco, A.; Rodríguez-Matellán, A.G.; Reis-Sobreiro, M.; Sáenz-Narciso, B.; Cabello, J.; Mohler, W.A.; Mollinedo, F. *Caenorhabditis elegans* as a platform to study the mechanism of action of synthetic antitumor lipids. *Cell. Cycle* **2014**, *13*, 3375–3389. [CrossRef] [PubMed]
46. Artal-Sanz, M.; de Jong, L.; Tavernarakis, N. *Caenorhabditis elegans:* A versatile platform for drug discovery. *J. Biotechnol.* **2006**, *1*, 1405–1418. [CrossRef]
47. Yang, L.S.; Liang, J.; Yao, G.H.; Chen, P.F.; Hou, Y.Y. 17beta-estradiol regulates the numbers, endocytosis, stimulative capacity and IL-10 secretion of mouse spleen dendritic cells. *Toxicol. Lett.* **2005**, *155*, 239–246. [CrossRef]
48. Shi, D.Z.; Zhang, Y.; Tian, Y. SLAMF1 promotes methotrexate resistance via activating autophagy in choriocarcinoma cells. *Cancer Manag. Res.* **2020**, *12*, 13427–13436. [CrossRef]
49. Li, M.Y.; Zhu, X.L.; Zhao, B.X.; Shi, L.; Wang, W.; Hu, W.; Qin, S.L.; Chen, B.H.; Zhou, P.H.; Qiu, B.; et al. Adrenomedullin alleviates the pyroptosis of Leydig cells by promoting autophagy via the ROS–AMPK–mTOR axis. *Cell Death Dis.* **2019**, *10*, 489. [CrossRef]
50. Radenkovic, S.; Konjevic, G.; Nikitovic, M.; Stojanovic-Rundic, S.; Plesinac-Karapandzic, v.; Milovic-Kovacevic, M.; Jurisic, V. Evaluation of Cyclin D1 expression by western blotting methods and immunohistochemistry in breast cancer patients. *J. BUON* **2021**, *26*, 475–482.
51. Lu, P. Inhibitory effects of hyperoside on lung cancer by inducing apoptosis and suppressing inflammatory response via caspase-3 and NF-kappaB signaling pathway. *Biomed. Pharmacother.* **2016**, *82*, 216–225. [CrossRef]
52. Zhuang, Z.H.; Zhao, Y.L.; Wu, Q.L.; Li, M.; Liu, H.C.; Sun, L.M.; Gao, W.; Wang, D.Y. Adverse effects from clenbuterol and ractopamine on nematode *Caenorhabditis elegans* and the underlying mechanism. *PLoS ONE* **2014**, *9*, e85482. [CrossRef]
53. Lipinski, C.A.; Lombardo, F.; Dominy, B.W.; Feeney, P.J. Experimental and computational approaches to estimate solubility and permeability in drug discovery and development settings. *Adv. Drug. Deliv. Rev.* **2001**, *46*, 3–26. [CrossRef]
54. Lee, J.H.; Ahn, J.; Kim, J.W.; Lee, S.G.; Kim, H.P. Flavonoids from the Aerial Parts of *Houttuynia Cordata* Attenuate Lung Inflflammation in Mice. *Arch. Pharm. Res.* **2015**, *38*, 1304–1311. [CrossRef] [PubMed]
55. Tian, L.; Shi, X.; Yu, L.; Zhu, J.; Ma, R.; Yang, X. Chemical Composition and Hepatoprotective Effects of Polyphenol-Rich Extract from *Houttuynia cordata* tea. *J. Agric. Food Chem.* **2012**, *60*, 4641–4648. [CrossRef]

56. Jones, G.S.; Baldwin, D.R. Recent Advances in the Management of Lung Cancer. *Clin. Med.* **2018**, *18*, s41–s46. [CrossRef] [PubMed]
57. Han, K.; Jin, C.; Chen, H.; Wang, P.P.; Yu, M.; Ding, K. Structural characterization and anti-A549 lung cancer cells bioactivity of a polysaccharide from *Houttuynia cordata*. *Int. J. Biol. Macromol.* **2018**, *120*, 288–296. [CrossRef] [PubMed]
58. Wang, D.; Noda, Y.; Zhou, Y.; Nitta, A.; Nabeshima, T.; Yu, Q.H. Effects of sodium houttuyfonate on phosphorylation of CaMK II, CREB and ERK 1/2 and expression of c-Fos in macrophages. *Int. Immunopharmacol.* **2004**, *4*, 1083–1088. [CrossRef]
59. Wang, W.Q.; Hu, X.Y.; Shen, P.S.; Zhang, N.S.; Fu, Y.H. Sodium houttuyfonate inhibits LPS-induced inflammatory response via suppressing TLR4/NF-κB signaling pathway in bovine mammary epithelial cells. *Microb. Pathog.* **2017**, *107*, 12–16. [CrossRef]
60. Zhu, Q.; Xu, X.L.; Liu, X.X.; Lin, J.B.; Kan, Y.; Zhong, Y.G.; Liu, F.H.; Xu, J.Q. Sodium houttuyfonate inhibits inflammation by blocking the MAPKs/NF-κB signaling pathways in bovine endometrial epithelial cells. *Res. Vet. Sci.* **2015**, *100*, 245–251. [CrossRef]
61. Omenn, G.S.; Guan, Y.; Menon, R. A new class of protein cancer biomarker candidates: Differentially expressed splice variants of ERBB2 (HER2/neu) and ERBB1 (EGFR) in breast cancer cell lines. *J. Proteom.* **2014**, *107*, 103–112. [CrossRef] [PubMed]
62. Choura, M.; Frikha, F.; Kharrat, N.; Aifa, S.; Rebaï, A. Investigating the function of three non-synonymous SNPs in EGFR gene: Structural modelling and association with breast cancer. *Protein J.* **2010**, *29*, 50–54. [CrossRef] [PubMed]
63. Shields, S.; Conroy, E.; O'Grady, T.; McGoldrick, A.; Connor, K.; Ward, M.P.; Useckaite, Z.; Dempsey, E.; Reilly, R.; Fan, Y.; et al. BAG3 promotes tumour cell proliferation by regulating EGFR signal transduction pathways in triple negative breast cancer. *Oncotarget* **2018**, *9*, 15673–15690. [CrossRef]
64. Park, H.S.; Jang, M.H.; Kim, E.J.; Kim, H.J.; Lee, H.J.; Kim, Y.J.; Kim, J.H.; Kang, E.; Kim, S.W.; Kim, I.A.; et al. High EGFR gene copy number predicts poor outcome in triple-negative breast cancer. *Mod. Pathol.* **2014**, *27*, 1212–1222. [CrossRef]
65. Nava, M.; Dutta, P.; Zemke, N.R.; Farias-Eisner, R.; Vadgama, J.V.; Wu, Y. Transcriptomic and ChIP-sequence interrogation of EGFR signaling in HER2+ breast cancer cells reveals a dynamic chromatin landscape and S100 genes as targets. *BMC Med. Genomics* **2019**, *12*, 32. [CrossRef]
66. Yanarojana, M.; Nararatwanchai, T.; Thairat, S.; Tancharoen, S. Antiproliferative activity and induction of apoptosis in human melanoma cells by *Houttuynia cordata* Thunb extract. *Anticancer Res.* **2017**, *37*, 6619–6628. [PubMed]
67. Zhou, N.N.; Tang, J.; Chen., W.D.; Feng, G.K.; Xie, B.F.; Liu, Z.C.; Yang, D.J.; Zhu, X.F. Houttuyninum, an active constituent of Chinese herbal medicine, inhibits phosphorylation of HER2/neu receptor tyrosine kinase and the tumor growth of HER2/neu-overexpressing cancer cells. *Life Sci.* **2012**, *90*, 770–775. [CrossRef] [PubMed]
68. Kim, I.S.; Kim, J.H.; Kim, J.S.; Yun, C.Y.; Kim, D.H.; Lee, J.S. The inhibitory effect of *Houttuynia cordata* extract on stem cell factor-induced HMC-1 cell migration. *J. Ethnopharmacol.* **2007**, *112*, 90–95. [CrossRef]
69. Duo, J.; Ying, G.G.; Wang, G.W.; Zhang, L. Quercetin inhibits human breast cancer cell proliferation and induces apoptosis via Bcl-2 and Bax regulation. *Mol. Med. Rep.* **2012**, *5*, 1453–1456.
70. Sakthivel, K.M.; Guruvayoorappan, C. Targeted inhibition of tumor survival, metastasis and angiogenesis by Acacia ferruginea mediated regulation of VEGF, inflammatory mediators, cytokine profile and inhibition of transcription factor activation. *Regul. Toxicol. Pharmacol.* **2018**, *95*, 400–411. [CrossRef]
71. Song, P.; Hai, Y.; Wang, X.; Zhao, L.H.; Chen, B.Q.; Cui, P.; Xie, Q.J.; Yu, L.; Li, Y.; Wu, Z.R.; et al. Realgar transforming solution suppresses angiogenesis and tumor growth by inhibiting VEGF receptor 2 signaling in vein endothelial cells. *Arch. Pharm. Res.* **2018**, *41*, 467–480. [CrossRef] [PubMed]
72. Kim, J.M.; Hwang, I.H.; Jang, I.S.; Kim, M.; Bang, I.S.; Park, S.J.; Chung, Y.J.; Joo, J.C.; Lee, M.G. *Houttuynia cordata* Thunb promotes activation of HIF-1A–FOXO3 and MEF2A pathways to induce apoptosis in human HepG2 hepatocellular carcinoma cells. *Integr. Cancer Ther.* **2017**, *16*, 360–372. [CrossRef]
73. Prommaban, A.; Kodchakorn, K.; Kongtawelert, P.; Banjerdpongchai, R. *Houttuynia cordata* Thunb fraction induces human leukemic Molt-4 cell apoptosis through the endoplasmic reticulum stress pathway. *Asian Pac. J. Cancer Prev.* **2012**, *13*, 1977–1981. [CrossRef]
74. Zhou, W.; Wu, Y.S.; Pan, M.; Liu, D.J.; Liu, B. Proliferation and migration of lung cancer could be inhibited by oxymatrine through the regulation for miR-520/VEGF. *Am. J. Chin. Med.* **2019**, *47*, 865–878. [CrossRef]
75. Sridhar, S.; Botbol, Y.; Macian, F.; Cuervo, A.M. Autophagy and disease: Always two sides to a problem. *J. Pathol.* **2012**, *226*, 255–273. [CrossRef]
76. Marsh, T.; Debnath, J. Autophagy suppresses breast cancer metastasis by degrading NBR1. *Autophagy* **2020**, *16*, 1164–1165. [CrossRef] [PubMed]
77. Aita, V.M.; Liang, X.H.; Murty, V.V.V.S.; Pincus, D.L.; Yu, W.P.; Cayanis, E.; Kalachikov, S.; Gilliam, T.C.; Levine, B. Cloning and genomic organization of Beclin 1, a candidate tumor suppressor gene on chromosome 17q21. *Genomics* **1999**, *59*, 59–65. [CrossRef] [PubMed]
78. Liang, X.H.; Jackson, S.; Seaman, M.; Brown, K.; Kempkes, B.; Hibshoosh, H.; Levine, B. Induction of autophagy and inhibition of tumorigenesis by beclin1. *Nature* **1999**, *402*, 672–676. [CrossRef]
79. Yue, Z.; Jin, S.; Yang, C.; Levine, A.J.; Heintz, N. Beclin1, an autophagy gene essential for early embryonic development, is a haploinsufficient tumor suppressor. *Proc. Natl. Acad. Sci. USA* **2003**, *100*, 15077–15082. [CrossRef]
80. Wang, S.; Wang, K.; Wang, H.Q.; Han, J.K.; Sun, H.K. Autophagy is essential for flavopiridol-induced cytotoxicity against MCF-7 breast cancer cells. *Mol. Med. Rep.* **2017**, *16*, 9715–9720. [CrossRef]

81. Wei, Y. EGFR-mediated Beclin 1 phosphorylation in autophagy suppression, tumor progression, and tumor chemoresistance. *Cell* **2013**, *154*, 1269–1284. [CrossRef] [PubMed]
82. Gschwind, A.; Fischer, O.M.; Ullrich, A. The discovery of receptor tyrosine kinases: Targets for cancer therapy. *Nat. Rev. Cancer* **2004**, *4*, 361–370. [CrossRef] [PubMed]
83. Muhsin, M.; Graham, J.; Kirkpatrick, P. Gefitinib. *Nat. Rev. Drug. Discov.* **2003**, *2*, 515–516. [CrossRef] [PubMed]
84. Mansour, N.I.; El-Sayed, S.M.; El-Gohary, N.S.; Abdel-Aziz, N.I.; El-Subbagh, H.I.; Ghaly, M.A. New phthalimide-based derivatives as EGFR-TK inhibitors: Synthesis, biological evaluation, and molecular modeling study. *Bioorg Chem.* **2022**, *127*, 105966. [CrossRef]
85. El-Gazzar, Y.I.; Ghaiad, H.R.; Kerdawy, A.M.E.; George, R.F.; Georgey, H.H.; Youssef, K.M.; El-Subbagh, H.I. New quinazolinone-based derivatives as DHFR/EGFR-TK inhibitors: Synthesis, molecular modeling simulations, and anticancer activity. *Arch. Pharm.* **2023**, *356*, e2200417. [CrossRef]
86. Markowicz, J.; Uram, Ł.; Sobich, J.; Mangiardi, L.; Maj, P.; Rode, W. Antitumor and anti-nematode activities of α-mangostin. *Eur. J. Pharmacol.* **2019**, *863*, 172678. [CrossRef] [PubMed]